Electronic Supplementary Information
Exploring Uracil Derivatives:
Synthesis, Crystal Structure Insights, and Antibacterial Activity

Susital Mal [a], Chris H. J. Franco[b*], Binay Kumar [a], Alexander M. Kirillov [b], and Subrata Das[a*]

* Corresponding authors

[a] *Department of Chemistry, National Institute of Technology Patna, Bihar 800005, India. subrataorgchem@gmail.com*

[b] *MINDlab: Molecular Design & Innovation Laboratory, Centro de Química Estrutural, Institute of Molecular Sciences, Instituto Superior Técnico, Universidade de Lisboa, Lisboa, Portugal. chris.franco@tecnico.ulisboa.pt*

Electronic Supplementary Information (ESI) contains: Additional discussion, experimental and structural details for compounds 1-4; FT-IR, UV-visible and NMR spectra; antibacterial activity and solubility data (Figures S3-S24, Tables S1-S9). CCDC 2306291-2306292 (PDF).

Index

Materials and Methods. All the reagents were purchased from Sigma-Aldrich, TCI (Tokyo Chemical Industry), Spectrochem, and Avra chemicals and used without further purification. All the solvents such as methanol, N,N-dimethylformamide (DMF), and N,N-dimethylformamidedimethylacetal (DMF-DMA) were purified before use. The Fourier Transform Infrared Spectroscopy (FT-IR) spectra was recorded on a Shimadzu Iraffinity-1s spectrophotometer (400-4000 cm^{-1}). The UV-visible spectra were measured on a Shimadzu UV-1780 spectrophotometer. Both ^{1}H and ^{13}C NMR spectra were recorded on a Bruker 400 MHz spectrometer at room temperature using DMSO-d_6 as a solvent and tetramethylsilane (TMS) as an internal standard.

Table S1. Crystal Data for Compounds **1**-**4**.

Compounds	**1**	**2**	**3**	**4**
Chemical formula	$C_8H_{12}N_4O_2{\cdot}H_2O$	$C_5H_5ClN_2O_2$	$C_7H_8N_2O_4{\cdot}2(H_2O)$	$C_4H_5N_3OS{\cdot}H_2O$
M_r	214.23	160.56	220.19	161.19
Crystal system, space group	Triclinic, *P-1*	Monoclinic, $P2_1/c$	Triclinic, *P-1*	Monoclinic, $C2/c$
Temperature (K)	293	297	293	298
a, *b*, *c* (Å)	8.0489 (9), 8.2275 (8), 8.8795 (9)	4.4654 (3), 15.9542 (10), 9.1808 (6)	5.1105 (6), 7.7802 (9), 13.1733 (13)	14.9108 (6), 7.6105 (3), 13.0084 (5)
α, β, γ (°)	65.458 (10), 78.475 (9), 73.773 (10)	-, 93.234 (4), -	77.211 (9), 89.735 (9), 76.363 (10)	-, 113.503 (2), -
V (Å^3)	511.22 (10)	653.02 (7)	495.76 (10)	1353.71 (9)
Z	2	4	2	8
Radiation type	Mo*K*α	Cu*K*α	Mo*K*α	Mo*K*α
μ (mm^{-1})	0.11	4.68	0.13	3.82
Data collection				
Diffractometer	SuperNova, Single source at offset/far, EosS2	Bruker axs kappa apex3 PHOTON II Diffractometer	SuperNova, Single source at offset/far, EosS2	Bruker D8 Venture Diffractometer with PHOTON II detector
T_{min}, T_{max}	0.728, 1.000	0.753, 0.454	0.744, 1.000	0.704, 1.000
No. of measured, independent and observed [$I > 2\sigma(I)$] reflections	3641, 2074, 1617	12752, 1289, 980	3759, 2029, 1668	14546, 1288, 1182
R_{int}	0.018	0.077	0.022	0.041
$(\sin\theta/\lambda)_{max}$ (Å^{-1})	0.625	0.618	0.625	0.610
Refinement				
$R[F^2 > 2\sigma(F^2)]$, $wR(F^2)$, *S*	0.051, 0.150, 1.06	0.097, 0.261, 1.12	0.059, 0.197, 1.12	0.031, 0.091, 1.11
No. of reflections	2074	1289	2029	1288
No. of parameters	154	92	150	95
No. of restraints	0	0	6	0
H-atom treatment	H-atom parameters constrained	H-atom parameters constrained	H atoms treated by a mixture of independent and constrained refinement	H-atom parameters constrained
$\Delta\rho_{max}$, $\Delta\rho_{min}$ (e Å^{-3})	0.24, −0.28	0.81, −0.34	0.39, −0.25	0.22, −0.22

Table S2. Energy Lattice ($E_{lattice}$) and Sublimation Enthalpy (ΔH_{sub}) Values for Uracil and Compounds **1-4**.

Compounds	$E_{lattice}$ (kJ mol^{-1})	ΔH_{sub} (kJ mol^{-1}) Calculated	ΔH_sub (kJ mol^{-1}) Experimental[#]
Uracil *	-133.1 ± 3.7	129.5 ± 3.7	131. ± 5
Uracil**	-142.3 ± 4.4	138.7 ± 4.4	131. ± 5
1*	-171.9 ± 5.1	170.1 ± 5.1	-
2*	-112.7 ± 3.2	109.3 ± 3.2	104. ± 6
3*	-176.6 ± 5.0	174.4 ± 5.0	-
4*	-182.5 ± 5.0	176.8 ± 5.0	-

Wave functions: *B3LYP/6-31G(d,p) and **HF/3-21G. [#] References: [S1], [S2] and [S3].

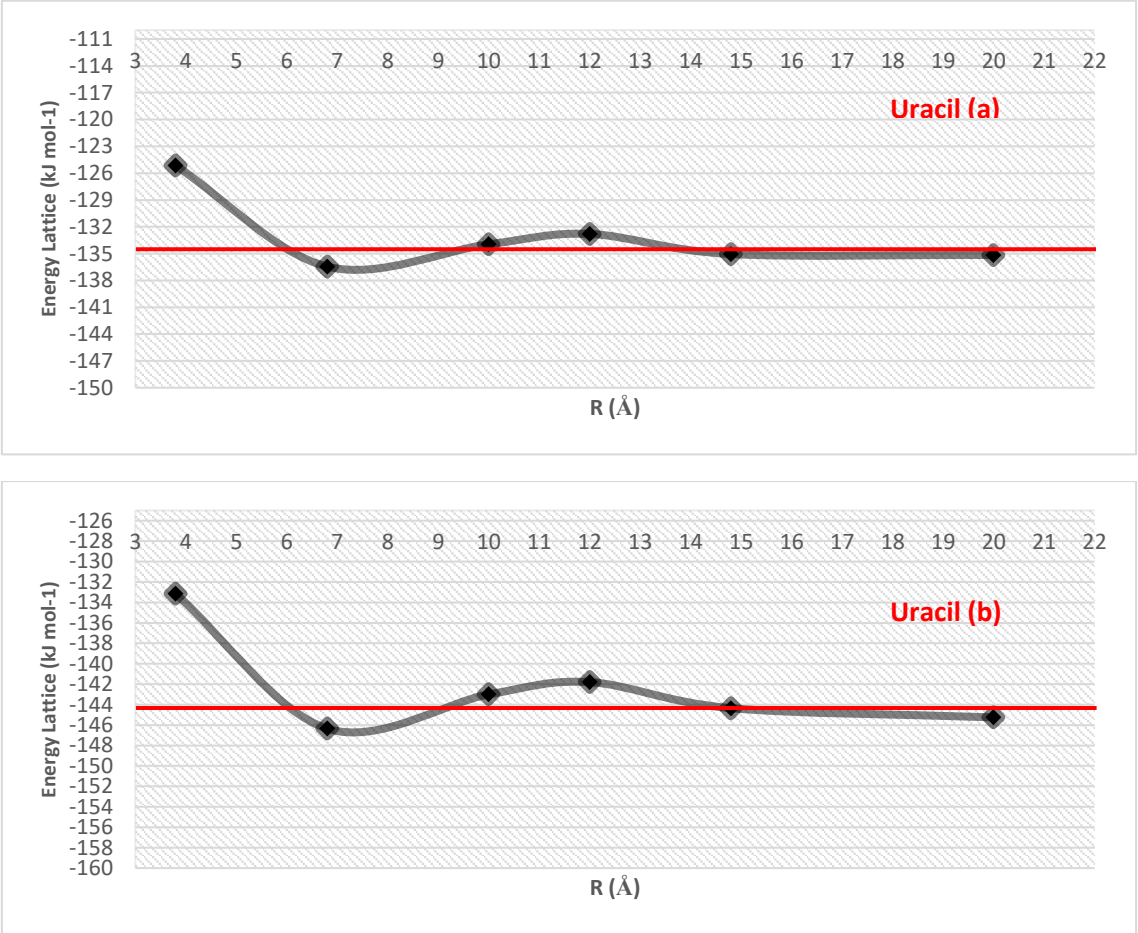

Figure S1. Lattice energy partial sums for uracil, plotted as a function of the center-of-mass distance between molecular pairs for distances ranging from 3 to 22 Å. (a) Based on B3LYP/6-31G(d,p) wave functions (more accurate). (b) Based on HF/3-21G wave functions.

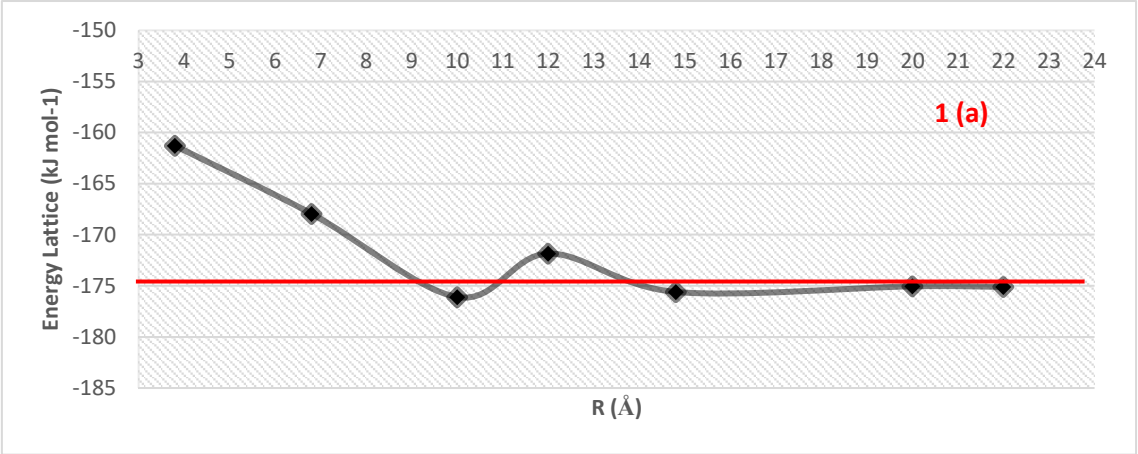
Energy Lattice (kJ mol-1)
-150
-155
-160
-165
-170
-175
-180
-185
3 4 5 6 7 8 9 10 11 12 13 14 15 16 17 18 19 20 21 22 23 24
R (Å)
1 (a)

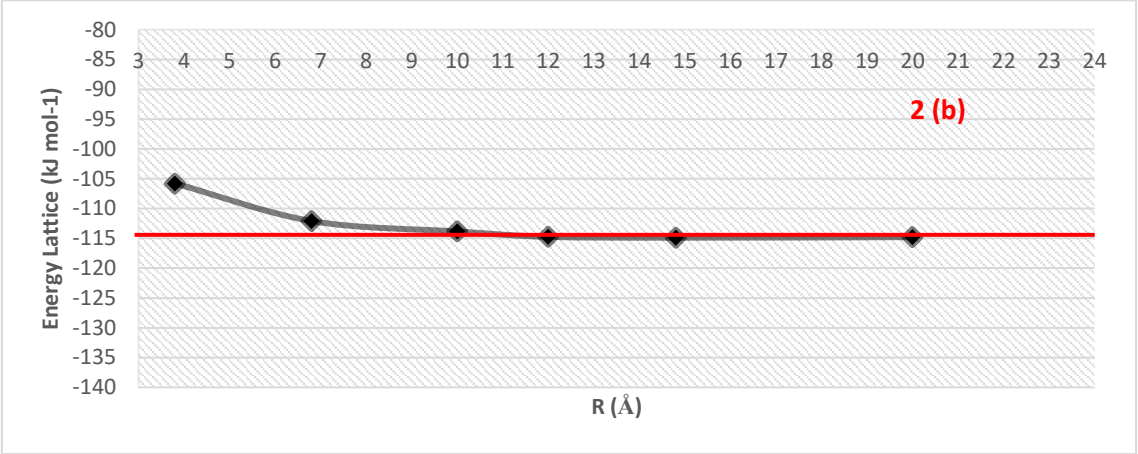
Energy Lattice (kJ mol-1)
-80
-85
-90
-95
-100
-105
-110
-115
-120
-125
-130
-135
-140
3 4 5 6 7 8 9 10 11 12 13 14 15 16 17 18 19 20 21 22 23 24
R (Å)
2 (b)

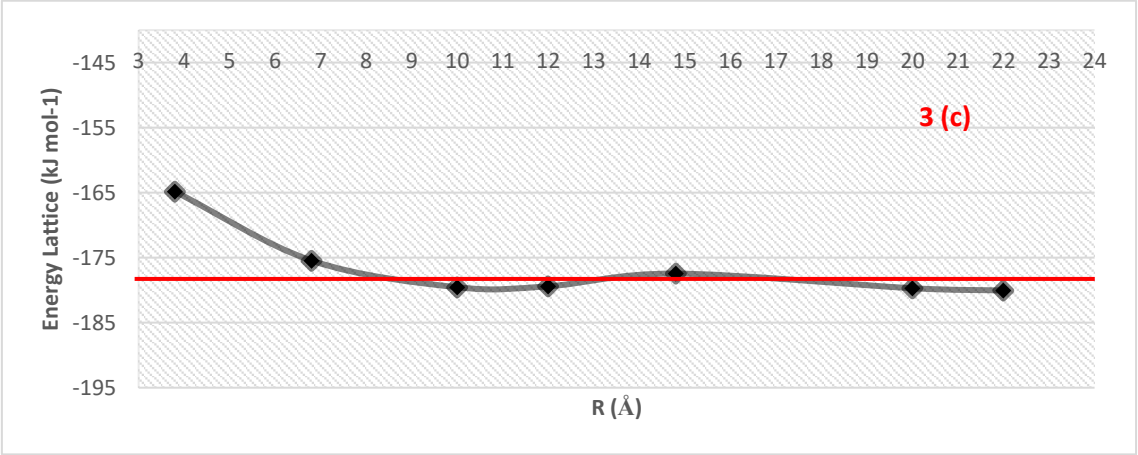
Energy Lattice (kJ mol-1)
-145
-155
-165
-175
-185
-195
3 4 5 6 7 8 9 10 11 12 13 14 15 16 17 18 19 20 21 22 23 24
R (Å)
3 (c)

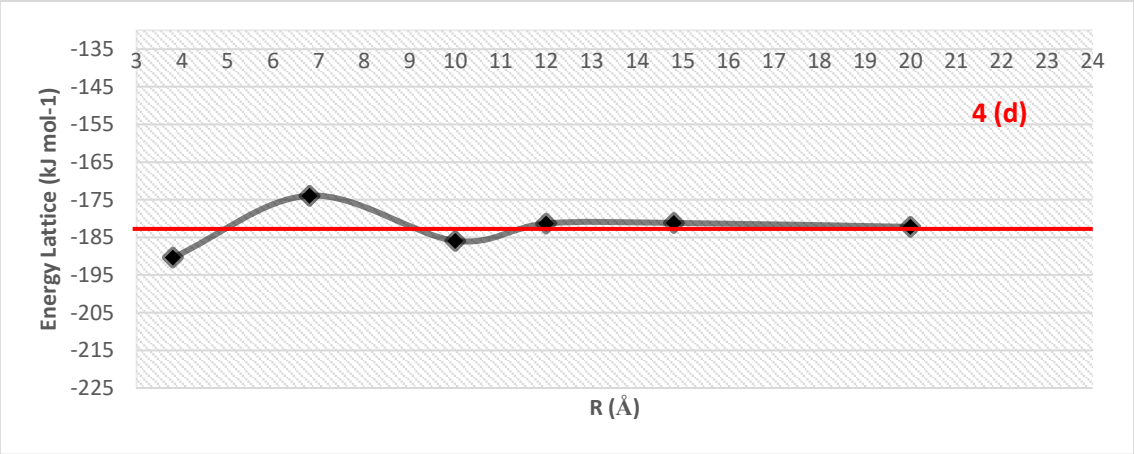

Figure S2. Lattice energy partial sums for compounds **1-4** (a-d), plotted as a function of the center-of-mass distance between molecular pairs for distances ranging from 3 to 22 Å, based on B3LYP/6-31G(d,p) wave functions.

FTIR Analysis: FTIR analysis was conducted to identify the presence of various functional groups within the compounds. In compound **1**, the absorption band at 3475 cm^{-1} is associated with the N-H group, while the two highly intense bands at 1652 and 1611 cm^{-1} correspond to $\nu(C{=}O)$ vibrations. For compound **2**, the presence of absorption bands at 3088, 1730, and 1704 cm^{-1} is attributed to the vibrational modes of the N-H and C=O groups, respectively. Similar absorption bands can be seen in compound **3**. In the case of compound **4**, the sharp and intense absorption peaks of the N-H and C=O groups are observed at 3420 and 1631 cm^{-1}, respectively (Table S3, Figures S3-S6). [S4, S5]

Table S3. Selected Infrared Absorption Bands for Compounds **1**-**4**.

Compound	FTIR bands (cm^{-1}) and Assignments	
	v(N-H)	*v(C=O)*
1	3475	1651, 1611
2	3088	1730, 1704
3	3176	1703
4	3420	1631

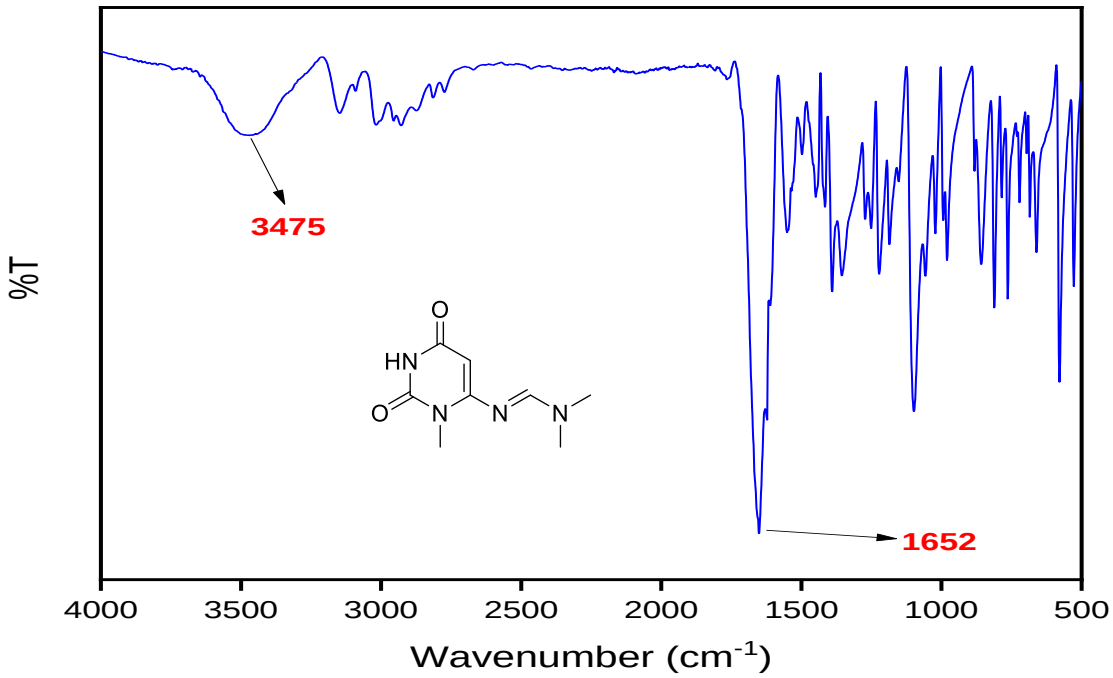

Figure S3. FT-IR spectrum of compound **1**.

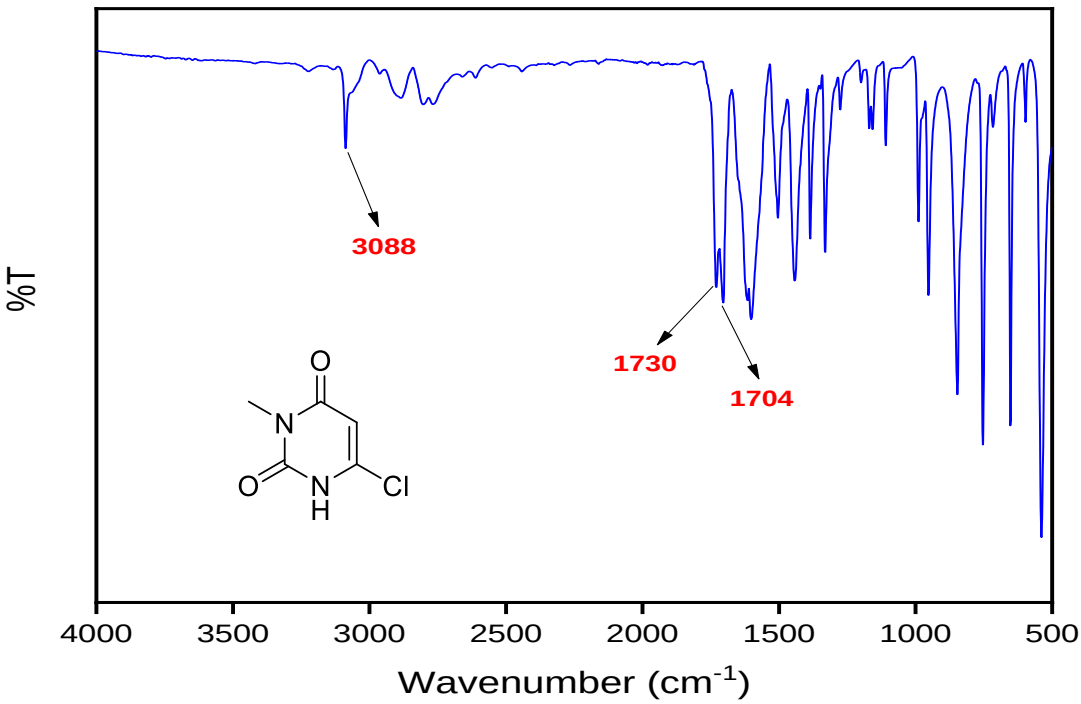

Figure S4. FT-IR spectrum of compound **2**.

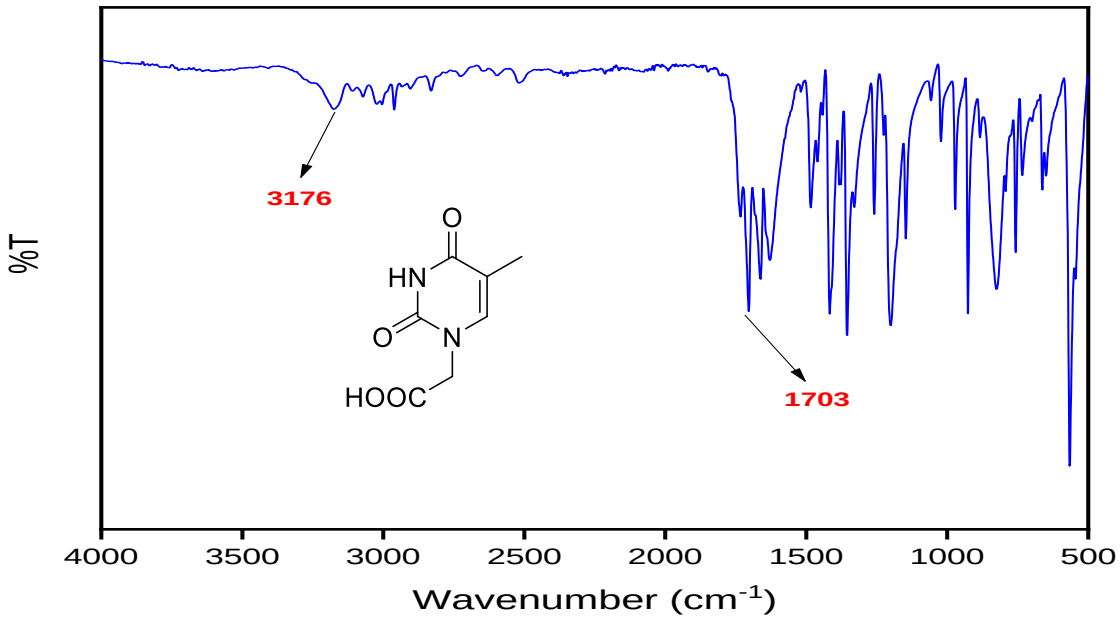

Figure S5. FT-IR spectrum of compound **3**.

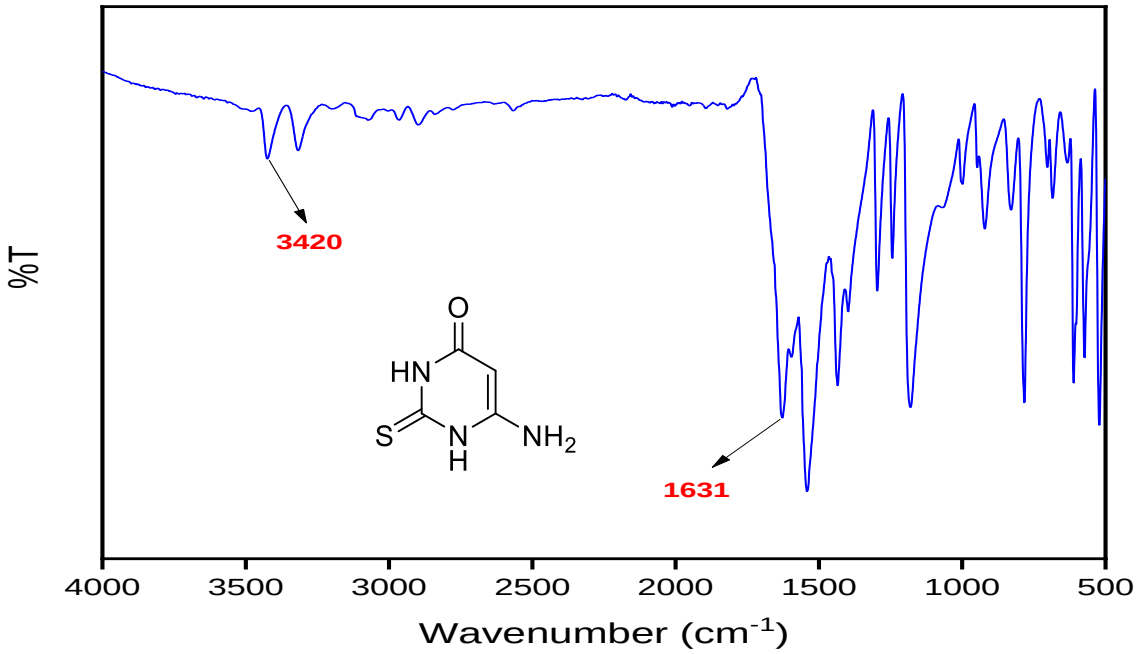

Figure S6. FT-IR spectrum of compound **4**.

Melting Point Determination and Purity Assessment: Melting point analyses were performed, and the results aligned with characterizations, indicating compound purity. Derivative 1 exhibits a melting range of 259–262 °C, and derivative 3 melts at 272–275 °C, further confirming the purity and homogeneity of both samples.

NMR Spectroscopy: For assessing structural features of the synthesized compounds **1** and **3** in the liquid state, the NMR spectroscopy was employed (Figures S7-S8). The ^{1}H NMR spectrum of **1** exhibits a number of signals due to H atom of the uracil ring (10.62 ppm), imine carbon proton (8.02 ppm), and the vinylic proton of the uracil ring (4.95 ppm). Additional signals at 3.20, 3.09, and 2.97 ppm correspond to the three methyl groups. In the ^{13}C NMR spectrum, signals at 163.61 and 161.24 ppm are assigned to the two carbonyl carbons of the uracil ring, while the peak at 156.26 ppm refers to the imine carbon. The vinylic carbon signal also appears at 82.71 ppm, while three additional peaks at 40.76, 34.86, and 29.10 ppm are associated with three methyl groups. In the ^{1}H NMR spectrum of **3**, the signals at 13.09 and 11.32 ppm are attributed to the carboxylic group (COOH) and amide group (=NH) protons, respectively. A signal at 7.48 ppm is assigned to vinylic carbon proton. The protons of N-CH_2 and C-CH_3 groups appear at 4.35 and 1.73 ppm, respectively. In the ^{13}C NMR spectrum, signals at 170.13, 164.83, and 151.45 ppm refer to carbon atom of COOH and carbonyl C atoms of the uracil ring, respectively. All observations are consistent with the X-ray results.

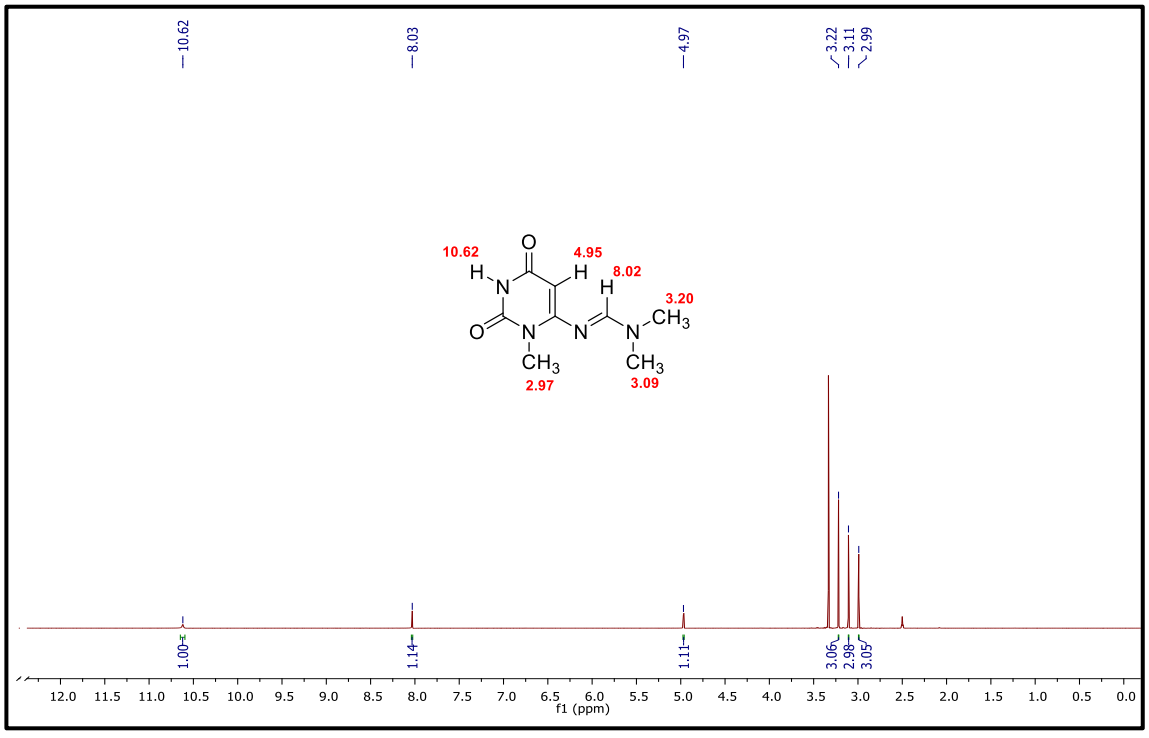

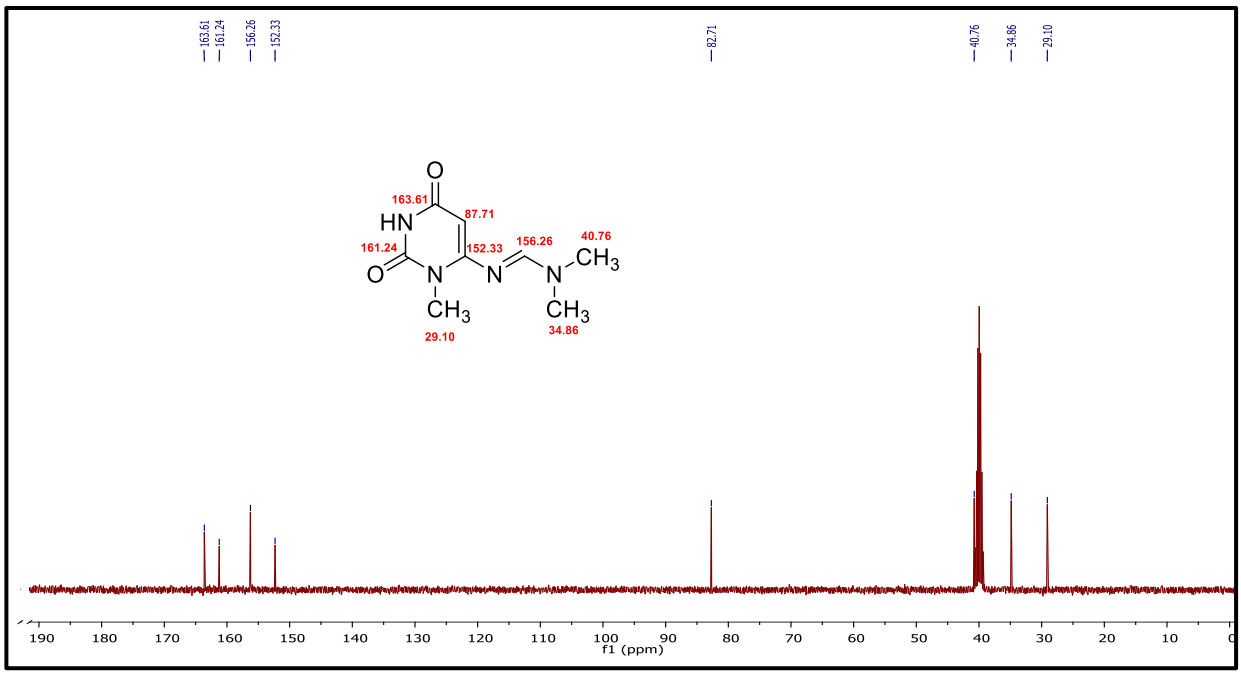

Figure S7. ^{1}H NMR and ^{13}C NMR spectra of compound **1**, (E)-N,N-dimethyl-N'-(3-methyl-2,6-dioxo-1,2,3,6-tetrahydropyrimidin-4-yl)formimidamide, in DMSO-d_6.

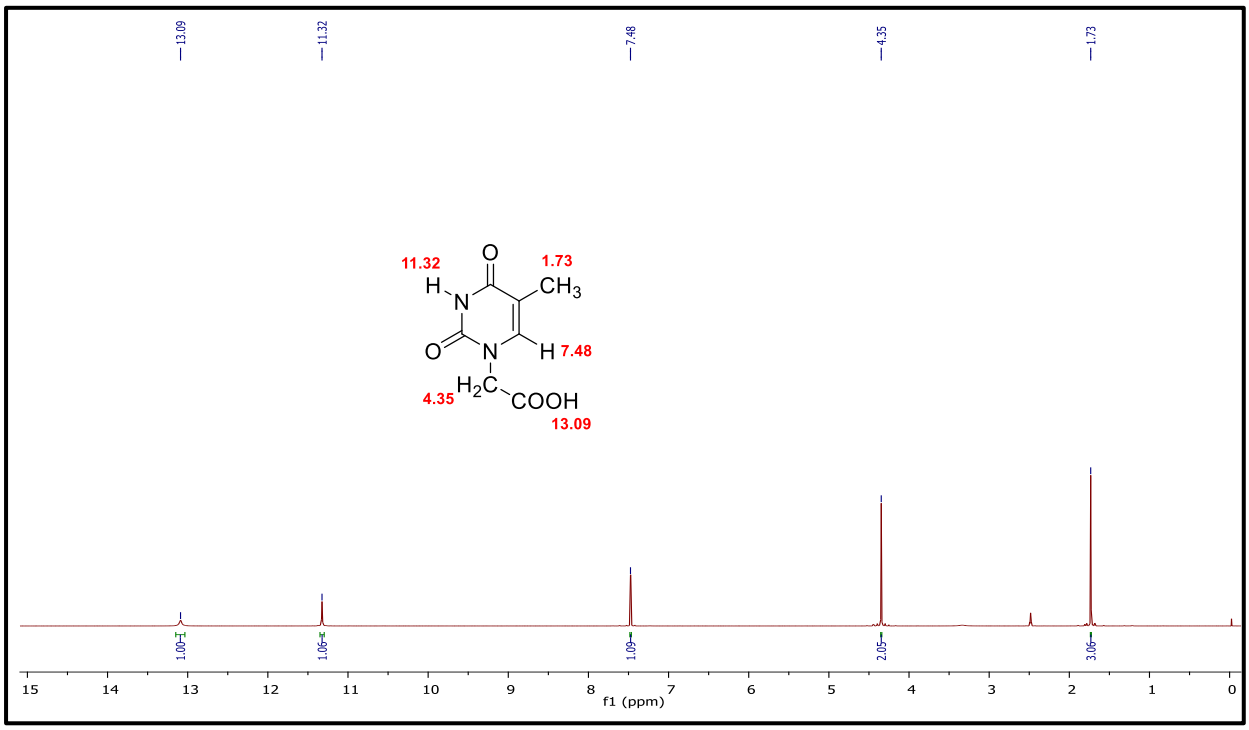

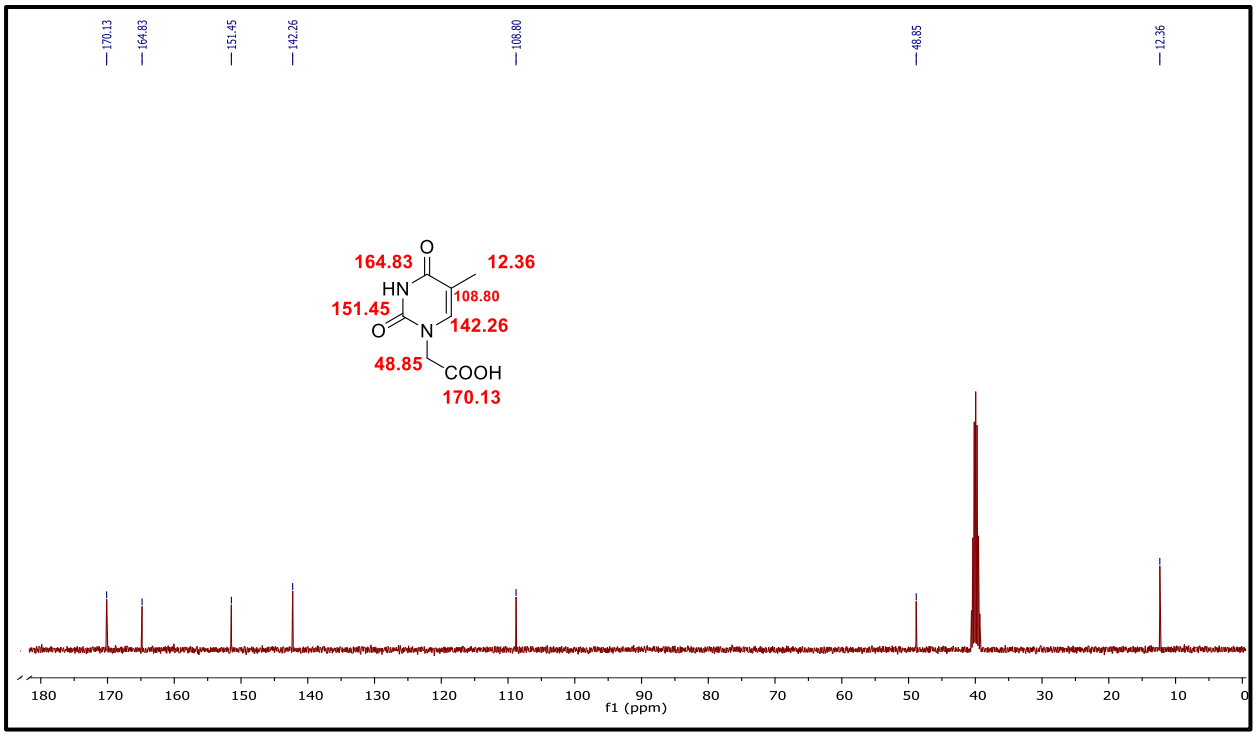

Figure S8. ^{1}H NMR and ^{13}C NMR spectra of compound **3**, 2-(5-methyl-2,4-dioxo-3,4-dihydropyrimidin-1(2H)-yl)acetic acid, in DMSO-d_6.

UV-visible Spectroscopy: Solution behavior of the obtained compounds was investigated in various protic (water, methanol and ethanol) and aprotic polar (acetonitrile, DMF and DMSO) solvents by UV-Vis spectroscopy (Table S4 and Figure S9). It was found that the λ_{max} (main absorbance band) in compounds **1**-**4** differs based on the type of solvent. For **1** and **4**, it is clear that λ_{max} value is influenced by their interaction with solvents, particularly due to H-bonding that can have an influence on the electronic structure of these compounds. [S6] In polar protic solvents, these interactions can lead to redshifts in the absorption spectra (234 to 245 nm for **1** and 275 to 288 nm for **4**). This means that λ_{max} is shifted toward longer wavelengths as H-bonds stabilize the excited state, altering the energy levels of electronic transitions. In polar aprotic solvents, compound **1** exhibits consistent redshift behavior, while conversely, in nonpolar solvents with reduced hydrogen bonding capacity, compound **4** demonstrates a blueshift in its λ_{max}. In addition, compounds **2** and **3** show blue shift behavior in all types of solvents.

Table S4. Absorption maxima (λ_{max}) of compounds **1**-**4** in different solvents.

Compound	Protic solvent			Aprotic solvent		
	Water	Methanol	Ethanol	Acetonitrile	DMF	DMSO
	λ_{max} (nm)	λ_{max} (nm)	λ_{max} (nm)	λ_{max} (nm)	λ_{max} (nm)	λ_{max} (nm)
1	234, 305	245, 306	244, 306	244, 302	305	306
2	328	326	322	312	288	263
3	272	272	267	266	235	235
4	275	288	282	269	234	235

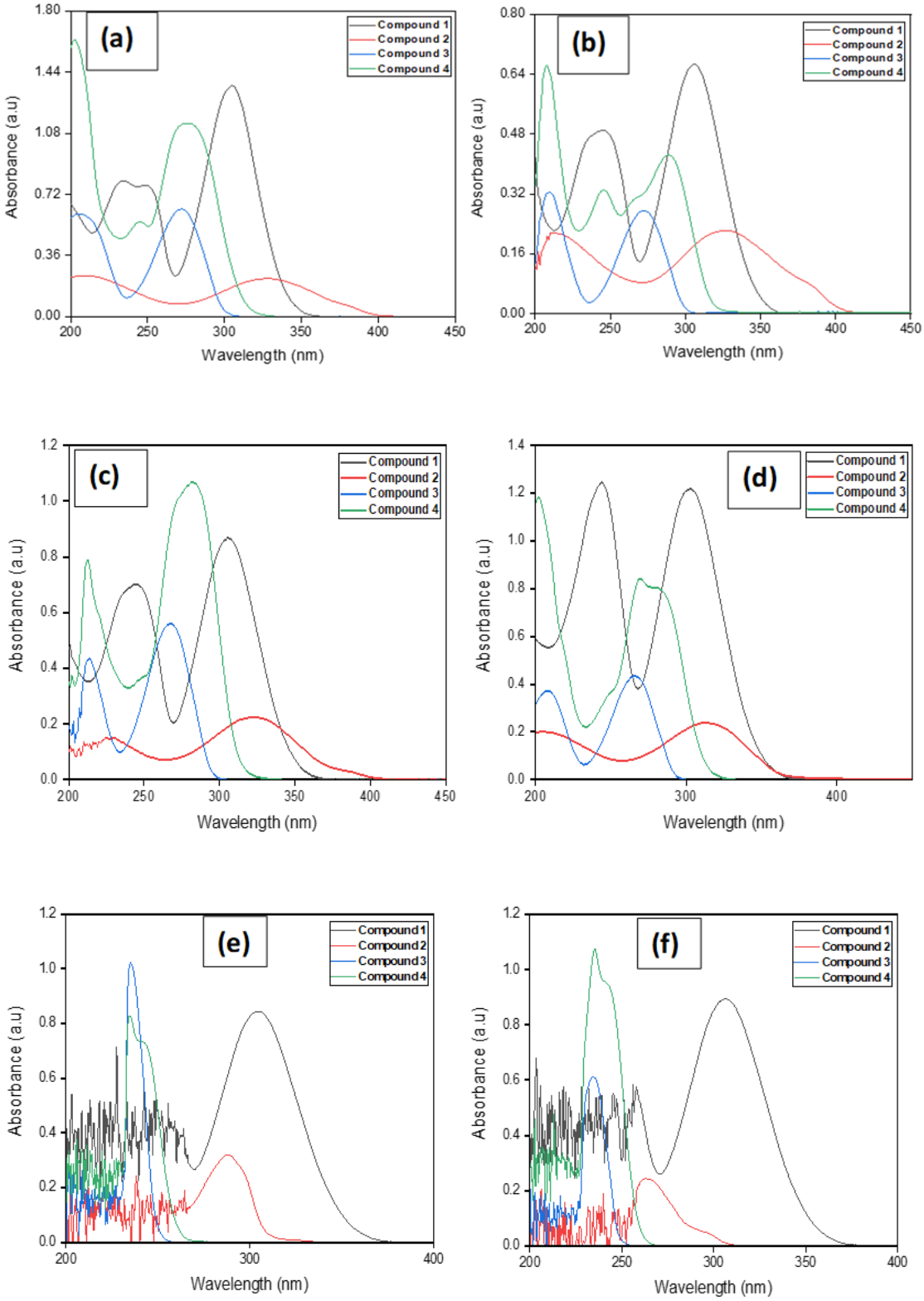

Figure S9. UV-visible spectra of compounds **1**-**4** in different solvents: (a) water, (b) methanol, (c) ethanol, (d) acetonitrile, (e) DMF, and (f) DMSO.

Table S5. Selected Bond Lengths (Å) in Compounds **1**-**4**.

	Compound 1		
O2—C2	1.249 (2)	N2—C4	1.392 (2)
O1—C1	1.216 (2)	N2—C1	1.381 (2)
N4—C5	1.315 (2)	N2—C8	1.468 (2)
N4—C6	1.453 (2)	N3—C4	1.364 (2)
N4—C7	1.449 (2)	N3—C5	1.306 (2)
N1—C1	1.373 (2)	C4—C3	1.373 (2)
N1—C2	1.380 (2)	C2—C3	1.408 (2)
	Compound 2		
Cl1—C2	1.708 (5)	N2—C1	1.376 (5)
N1—C2	1.364 (6)	N2—C4	1.386 (5)
N1—C1	1.372 (6)	N2—C5	1.467 (6)
O2—C4	1.245 (5)	C2—C3	1.341 (6)
O1—C1	1.214 (5)	C3—C4	1.421 (7)
	Compound 3		
O2—C2	1.236 (3)	O4—C7	1.299 (3)
O1—C1	1.223 (3)	O3—C7	1.209 (3)
N1—C2	1.381 (3)	C2—C3	1.435 (3)
N1—C1	1.369 (3)	C4—C3	1.343 (3)
N2—C1	1.370 (3)	C7—C6	1.511 (4)
N2—C4	1.374 (3)	C3—C5	1.502 (3)
N2—C6	1.460 (3)		
	Compound 4		
S1—C1	1.6744 (17)	N2—C4	1.371 (2)
O1—C2	1.253 (2)	C4—N3	1.335 (2)
N1—C1	1.348 (2)	C4—C3	1.378 (2)
N1—C2	1.387 (2)	C2—C3	1.395 (2)
C1—N2	1.354 (2)		

Table S6. Selected Bond Angles (°) in Compounds **1**-**4**.

	Compound 1		
C5—N4—C6	121.28 (15)	C3—C4—N2	118.99 (15)
C5—N4—C7	121.31 (14)	O1—C1—N1	121.42 (16)
C7—N4—C6	117.31 (14)	O1—C1—N2	122.69 (16)
C1—N1—C2	125.81 (14)	N1—C1—N2	115.88 (14)
C4—N2—C8	121.50 (14)	O2—C2—N1	118.66 (15)
C1—N2—C4	122.17 (14)	O2—C2—C3	125.92 (15)
C1—N2—C8	116.32 (13)	N1—C2—C3	115.40 (15)
C5—N3—C4	118.47 (14)	C4—C3—C2	121.69 (15)
N3—C4—N2	112.97 (14)	N3—C5—N4	122.01 (15)
N3—C4—C3	128.04 (14)		
	Compound 2		
C2—N1—C1	122.9 (4)	C4—C3—H3	120.9
C1—N2—C4	124.6 (4)	N1—C1—N2	114.8 (4)
C1—N2—C5	116.6 (4)	O1—C1—N1	121.6 (4)
C4—N2—C5	118.8 (4)	O1—C1—N2	123.6 (4)
N1—C2—Cl1	115.0 (3)	O2—C4—N2	118.9 (4)
C3—C2—Cl1	122.8 (4)	O2—C4—C3	123.8 (4)
C3—C2—N1	122.2 (4)	N2—C4—C3	117.4 (4)
C2—C3—C4	118.2 (4)		
	Compound 3		
C2—N1—H1	116.8	O1—C1—N2	122.2 (2)
C1—N1—C2	126.5 (2)	N1—C1—N2	115.18 (19)
C1—N2—C4	121.2 (2)	C3—C4—N2	123.4 (2)
C1—N2—C6	117.0 (2)	O4—C7—C6	111.9 (2)
C4—N2—C6	121.8 (2)	O3—C7—O4	124.7 (2)
C7—O4—H4	109.5	O3—C7—C6	123.4 (2)
O2—C2—N1	119.5 (2)	C2—C3—C5	118.7 (2)
O2—C2—C3	124.9 (2)	C4—C3—C2	118.0 (2)
N1—C2—C3	115.6 (2)	C4—C3—C5	123.3 (2)
O1—C1—N1	122.6 (2)	N2—C6—C7	111.2 (2)
	Compound 4		
C1—N1—C2	124.81 (14)	N3—C4—N2	116.74 (15)
N1—C1—S1	122.43 (13)	N3—C4—C3	124.26 (16)
N1—C1—N2	115.87 (15)	O1—C2—N1	117.64 (15)
N2—C1—S1	121.70 (13)	O1—C2—C3	125.39 (16)
C1—N2—C4	123.71 (14)	N1—C2—C3	116.95 (14)
N2—C4—C3	118.99 (15)	C4—C3—C2	119.60 (16)

Table S7. Hydrogen-bond Geometry (Å, °) in Compounds **1**-**4**.

D—H···A	D—H	H···A	D···A	D—H···A
		Compound 1		
N1—H1···O2^{i}	0.86	2.01	2.8658(19)	175.8
C5—H5···O3^{ii}	0.93	2.56	3.464(5)	164.6
C5—H5···O3A^{ii}	0.93	2.65	3.491(6)	149.9
O3—H3A···O3^{ii}	0.85	1.81	2.637(11)	164.4
O3—H3B···O2	0.85	2.11	2.956(5)	173.3
O3A—H3AA···O2	0.85	1.98	2.827(6)	175.5
Symmetry codes: ***(i)*** *−x+1, −y+2, −z;* ***(ii)*** *−x, −y+2, −z+1.*				
		Compound 2		
N1—H1···O2^{i}	0.86	1.93	2.785(5)	179.1
C3—H3···O1^{ii}	0.93	2.41	3.290(5)	157.0
C5—H5A···O1^{iii}	0.96	2.72	3.440(6)	132.5
Symmetry codes: ***(i)*** *x−1, −y+1/2, z−1/2;* ***(ii)*** *x+1, −y+1/2, z+1/2; (iii) −x, −y, −z.*				
		Compound 3		
O5—H5D···O6^{i}	0.882(19)	1.886(19)	2.766(3)	176(4)
O5—H5E···O3	0.859(18)	1.98(2)	2.790(3)	156(4)
N1—H1···O2^{ii}	0.86	2.00	2.860(3)	178.3
O6—H6C···O1^{iii}	0.854(19)	2.004(19)	2.858(3)	178(4)
O6—H6D···O2^{iv}	0.865(18)	2.16(3)	2.917(3)	146(4)
O4—H4···O5^{v}	0.82	1.80	2.614(3)	170.0
C4—H4A···O5^{iii}	0.93	2.52	3.376(3)	152.7
Symmetry codes: ***(i)*** *x, y+1, z;* ***(ii)*** *−x+1, −y+1, −z+2;* ***(iii)*** *x−1, y, z;* ***(iv)*** *−x, −y+1, −z+2;* ***(v)*** *−x+1, −y+2, −z+1.*				
		Compound 4		
O2—H2A···O1	0.85	1.92	2.7632(19)	173.1
O2—H2B···S1^{i}	0.85	2.69	3.4889(15)	158.1
N1—H1···O2^{ii}	0.86	1.99	2.8528(19)	176.7
N2—H2···O1^{iii}	0.86	1.95	2.7364(17)	151.2
N3—H3A···O1^{iii}	0.86	2.48	3.136(2)	133.2
N3—H3B···O2^{iv}	0.86	2.30	3.109(2)	157.7
C3—H3···O2^{iv}	0.93	2.66	3.413(2)	138.6
Symmetry codes: ***(i)*** *−x+3/2, −y+1/2, −z+1;* ***(ii)*** *−x+3/2, y+1/2, −z+1/2;* ***(iii)*** *x, −y+1, z+1/2;* ***(iv)*** *−x+1, y, −z+1/2.*				

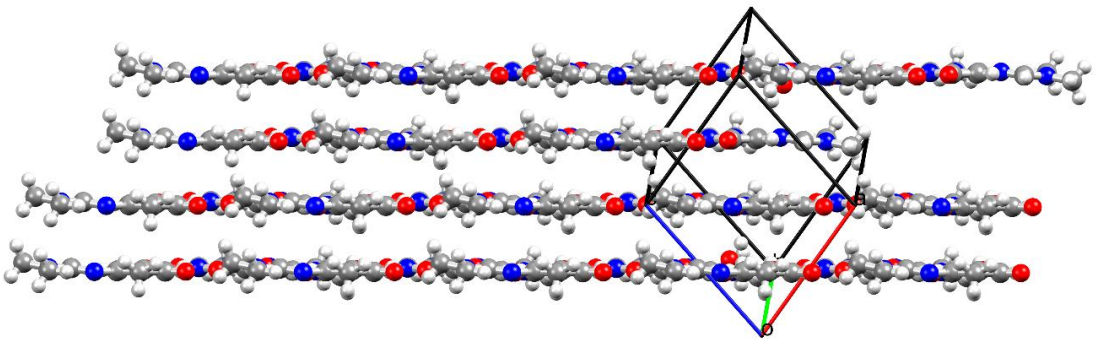

Figure S10. Representation of independent 1D supramolecular chains in **1** stabilized by long-range H-bonding interactions.

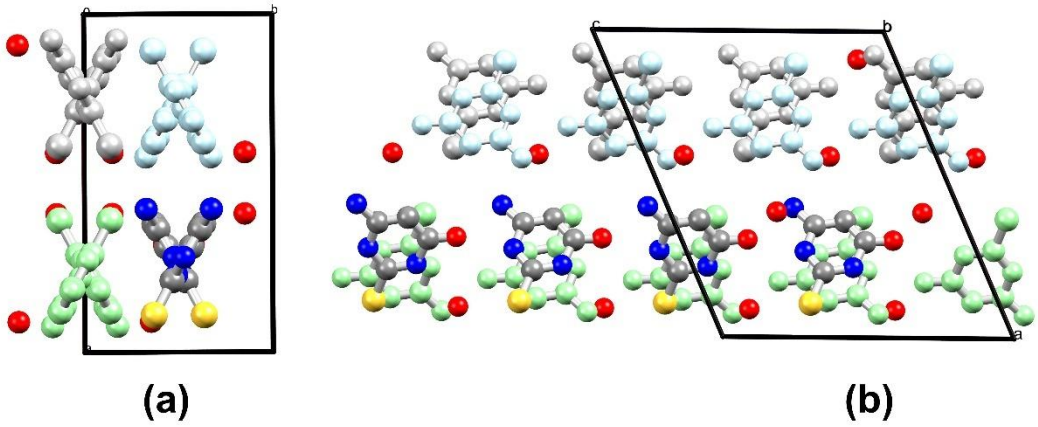

Figure S11. Representation of independent 1D supramolecular chains in **4** connected by H-bonds from water molecules. Views are (a) along the *c*-axis and (b) along the *b*-axis. Hydrogen atoms were omitted for clarity.

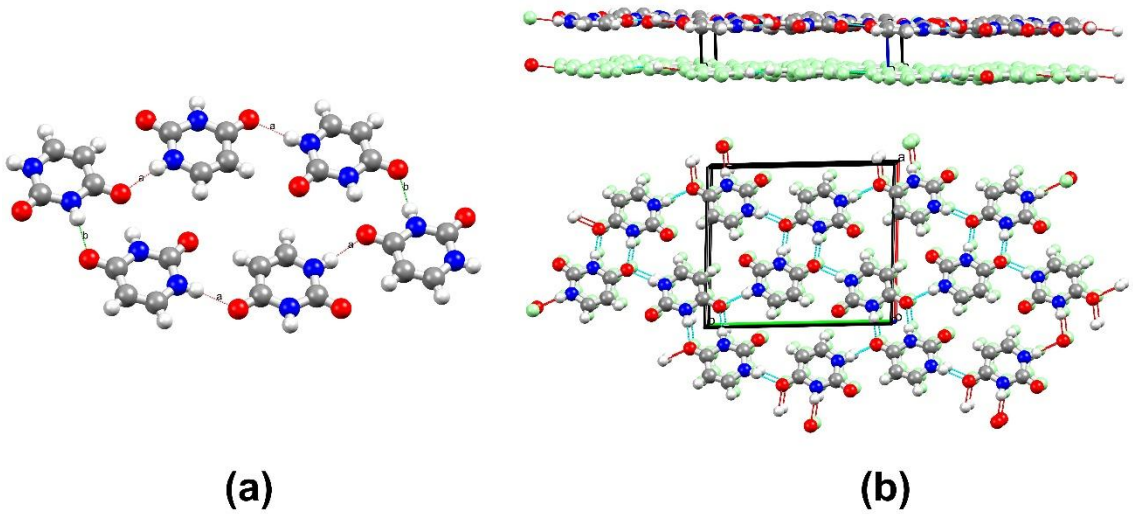

Figure S12. Representation of main $R_6^6(32)$ *synthons* in (a) for uracil structure. In (b) 2D sheets stacked representation along ***c***-axis (on top) and long-range interactions from pyrimidinone rings (on bottom) in ***ab***-plane.

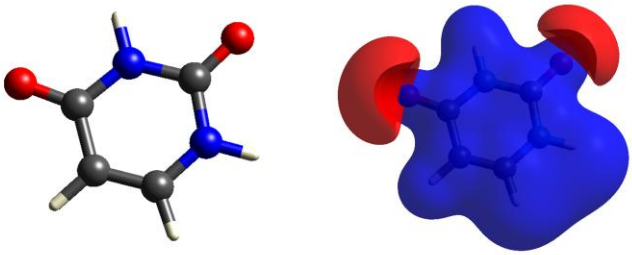

Figure S13. Molecular electrostatic potential isosurfaces in the crystal structure of uracil. The electron density surface drawn at ±0.05 a.u. contour. The quantum mechanical proprieties are derived from B3LYP/6-31G(d,p) wave functions.

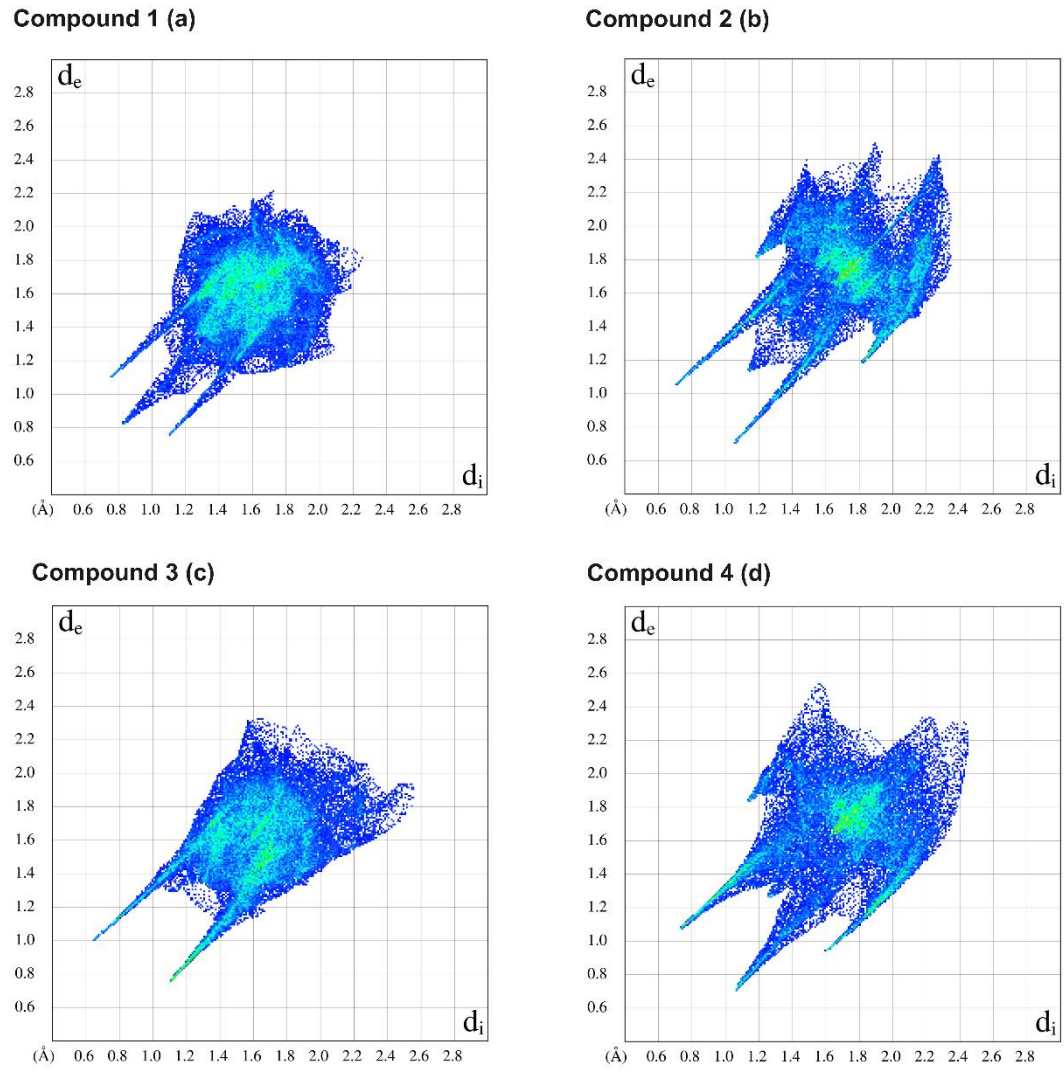

Figure S14. Details for 2D fingerprint plots of main contacts for compounds **1-4**.

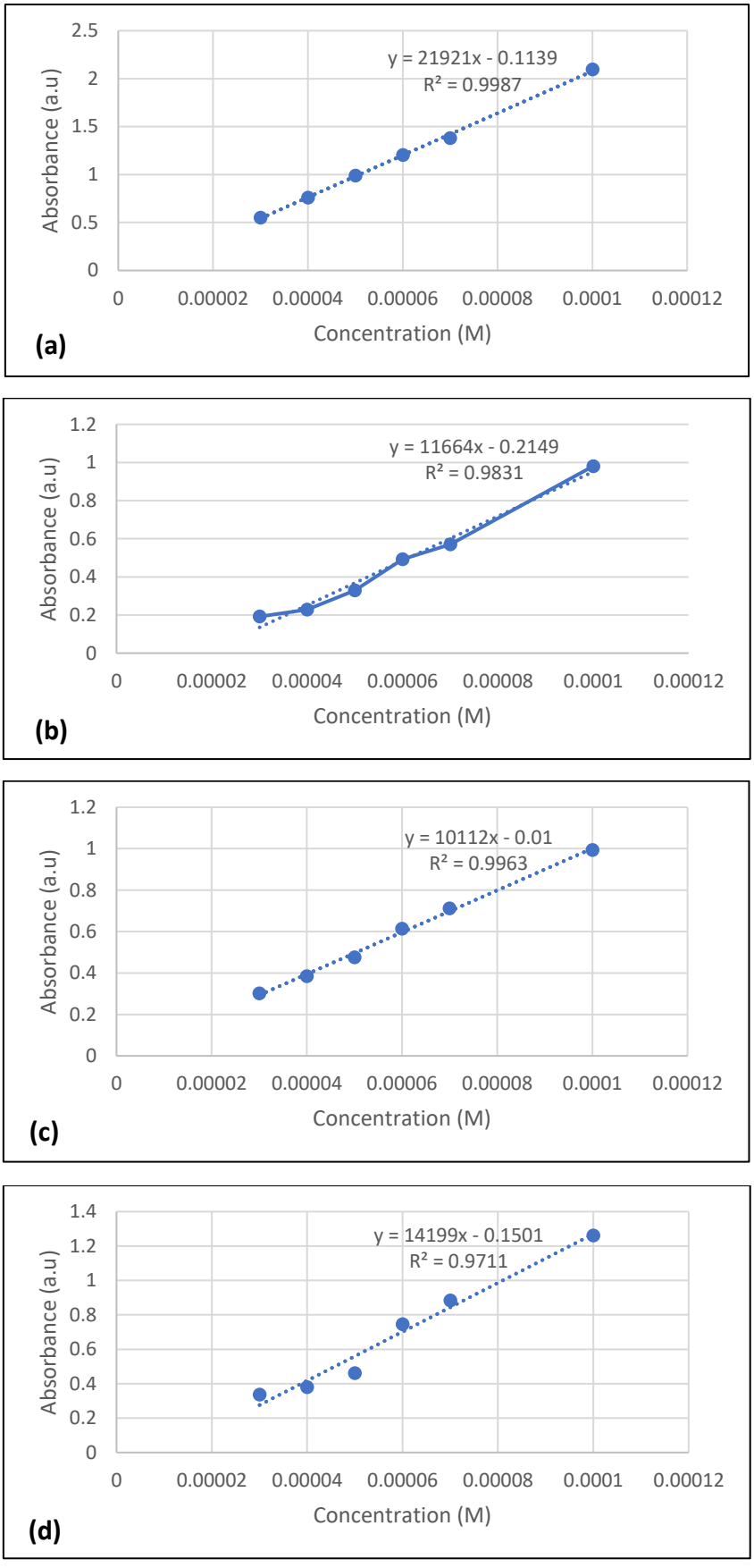

Figure S15. Calibration curve of absorbance *vs.* concentration for compounds **1**-**4** (a-d) in water.

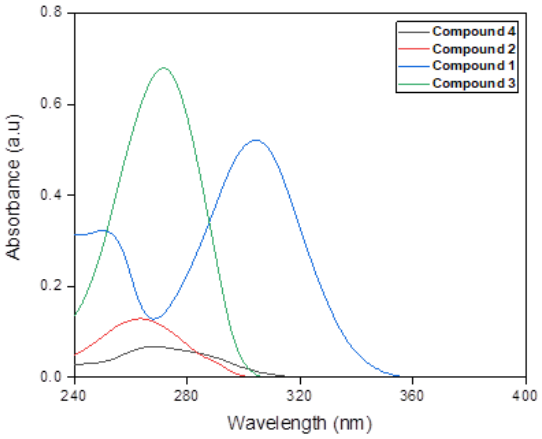

Figure S16. UV-visible spectra of compound **1**-**4** after stirring for 24 h in water.

Table S8. Inhibition Activity (%) for Compounds **1**-**4** against *E. coli*.

µg mL^{-1}	SET 1	SET 2	SET 3	N_{Total}	Mean	SD	SEM	Median	% inhibition
					Compound 1				
0	1.012	0.987	0.994	3	0.997667	0.012897	0.007446	0.994	
5.6	0.857	0.798	0.805	3	0.82	0.032234	0.01861	0.805	17.81
					Compound 2				
0	0.973	1.118	1.003	3	1.031333	0.07654	0.04419	1.003	
4.7	0.898	0.867	0.837	3	0.867333	0.030501	0.01761	0.867	15.90
					Compound 3				
0	0.997	0.983	1.127	3	1.035667	0.079406	0.045845	0.997	
12.5	0.735	0.693	0.713	3	0.713667	0.021008	0.012129	0.713	31.09
					Compound 4				
0	1.025	1.112	1.023	3	1.053333	0.050817	0.029339	1.025	
2.2	0.937	0.917	0.897	3	0.917	0.02	0.011547	0.917	12.94

Table S9. Inhibition Activity (%) for Compounds **1**-**4** against *S. aureus*.

µg mL^{-1}	SET 1	SET 2	SET 3	N_{Total}	Mean	SD	SEM	Median	% inhibition
					Compound 1				
0	1.021	1.107	1.153	3	1.093667	0.067002	0.038684	1.107	
5.6	0.912	0.958	0.987	3	0.952333	0.03782	0.021835	0.958	12.92
					Compound 2				
0	1.118	0.987	1.026	3	1.043667	0.067263	0.038834	1.026	
4.7	1.003	0.912	1.114	3	1.009667	0.101165	0.058408	1.003	3.26
					Compound 3				
0	0.993	1.012	0.976	3	0.993667	0.018009	0.010398	0.993	
12.5	0.927	0.891	0.952	3	0.923333	0.030665	0.017704	0.927	7.08
					Compound 4				
0	1.025	1.007	0.997	3	1.009667	0.014189	0.008192	1.007	
2.2	1.047	0.993	0.925	3	0.988333	0.061134	0.035296	0.993	2.11

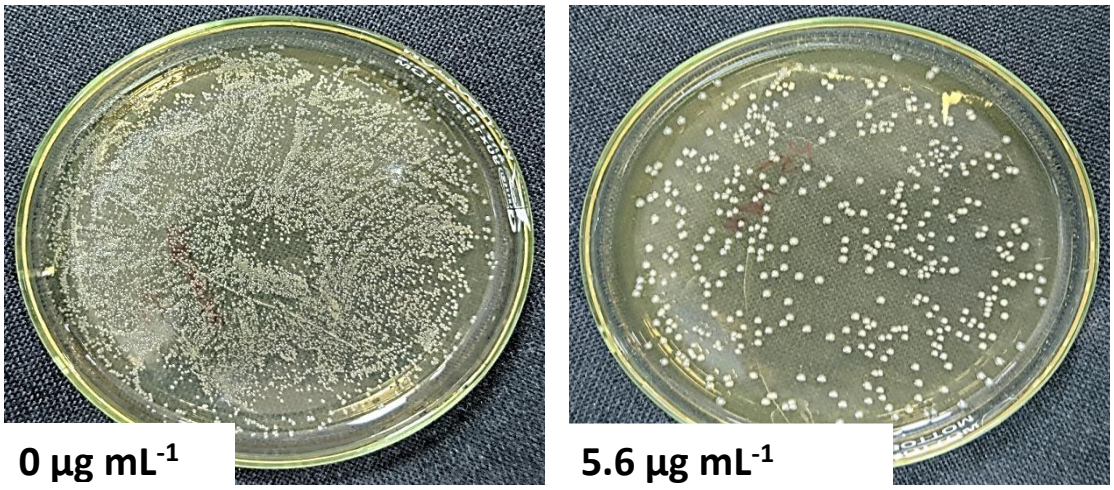

Figure S17. Images of Petri dishes revealing the antibacterial activity of **1** against *E. coli*.

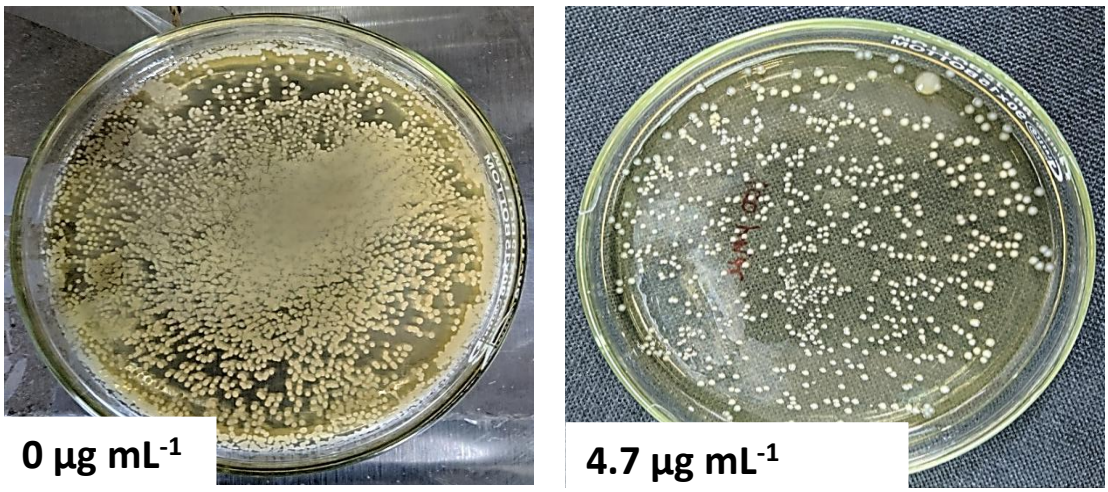

Figure S18. Images of Petri dishes revealing the antibacterial activity of **2** against *E. coli*.

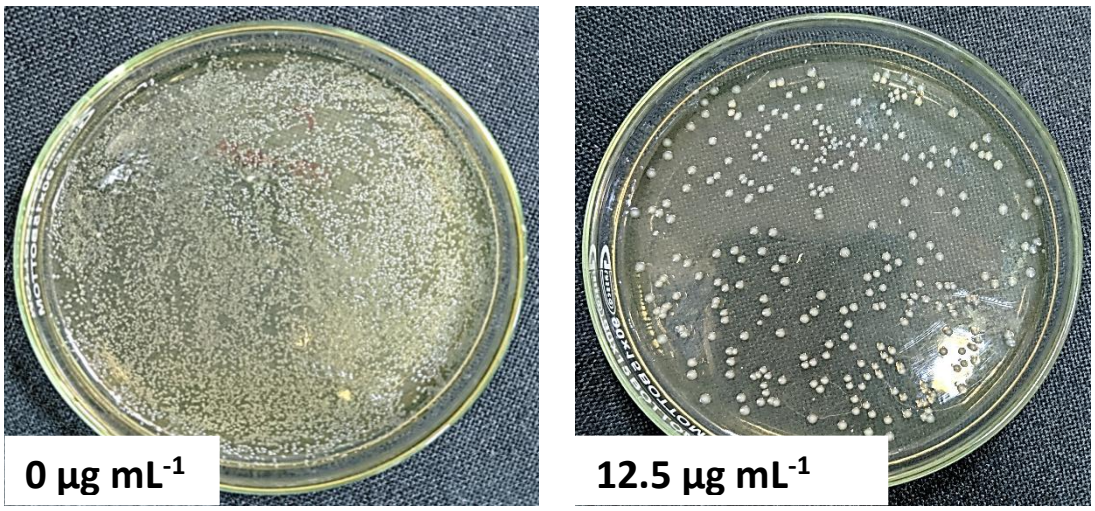

Figure S19. Images of Petri dishes revealing the antibacterial activity of **3** against *E. coli*.

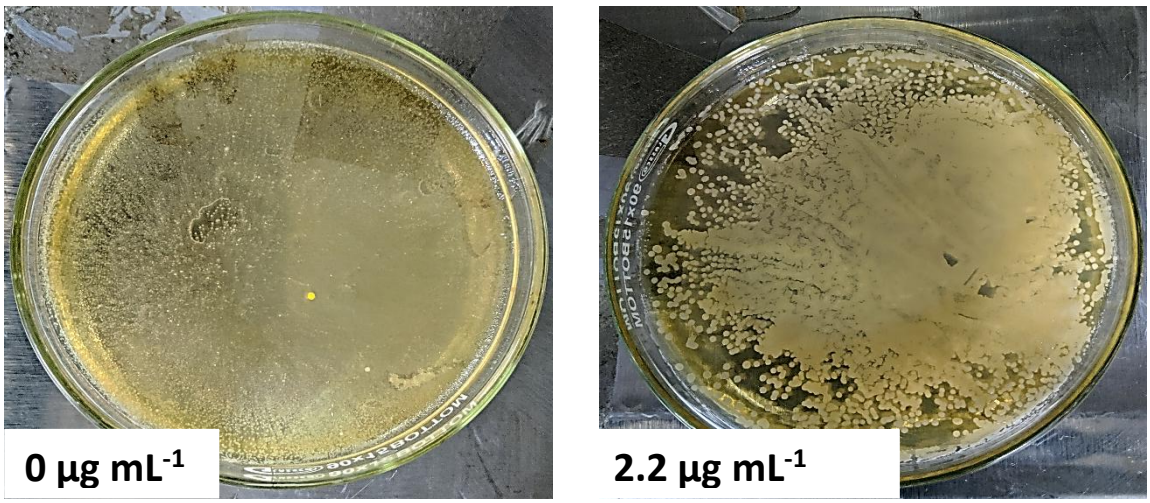

Figure S20. Images of Petri dishes revealing the antibacterial activity of **4** against *E. coli*.

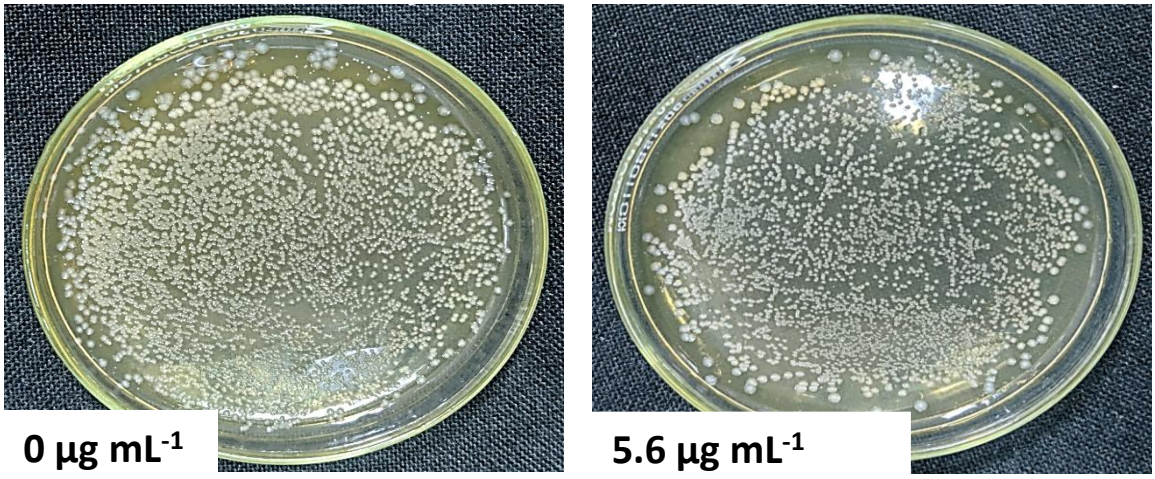

Figure S21. Images of Petri dishes revealing the antibacterial activity of **1** against *S. aureus*.

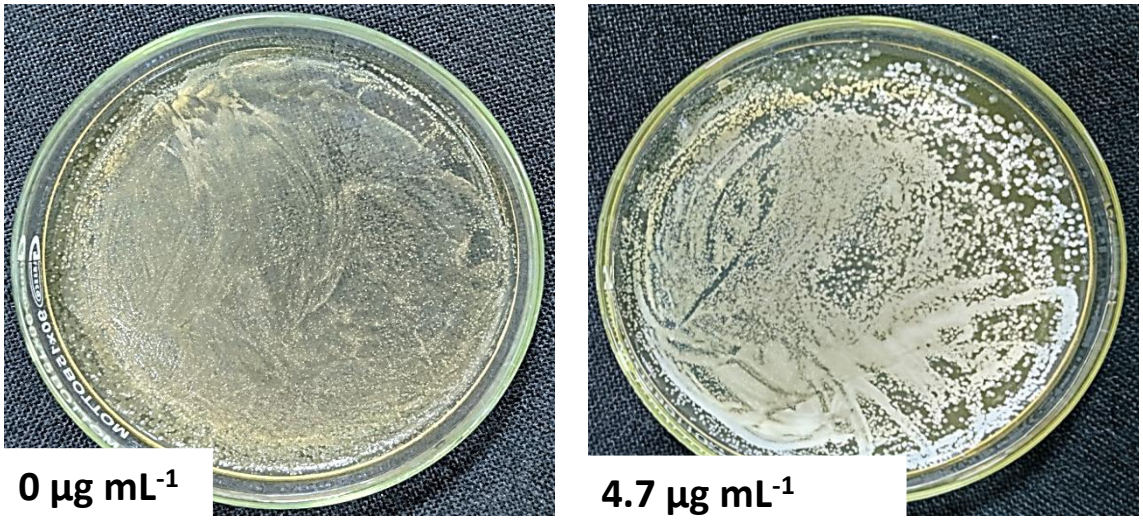

Figure S22. Images of Petri dishes revealing the antibacterial activity of **2** against *S. aureus*.

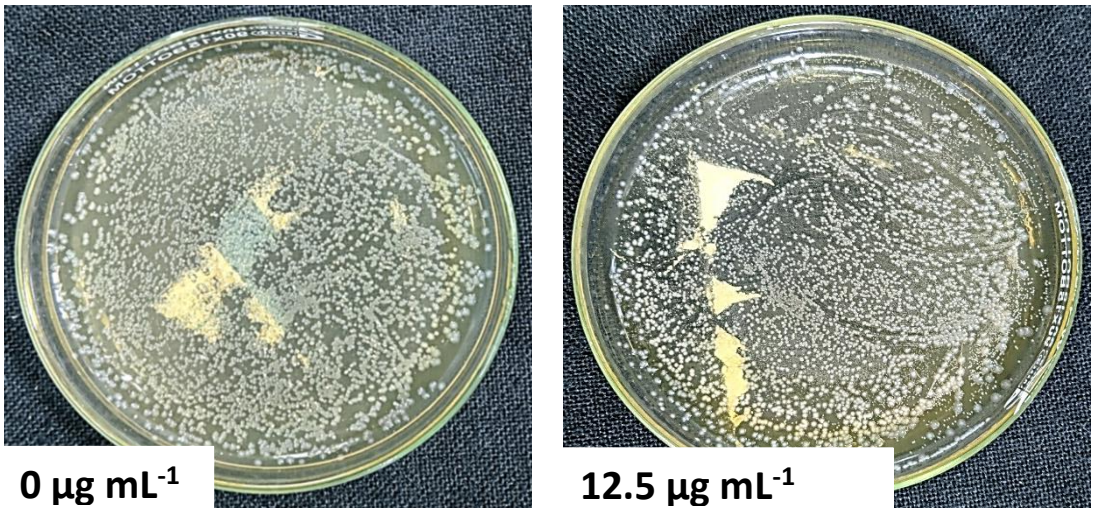

Figure S23. Images of Petri dishes revealing the antibacterial activity of **3** against *S. aureus*.

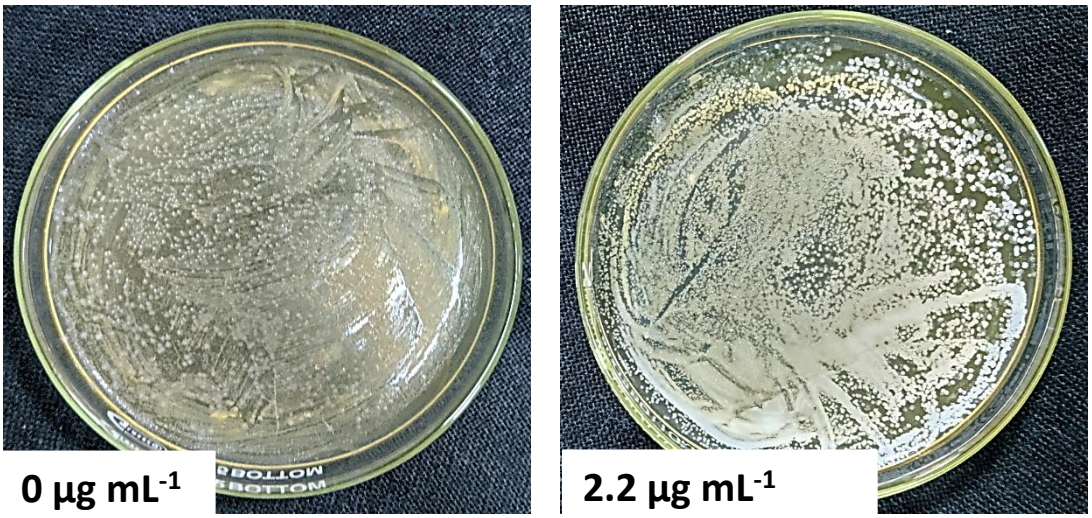

Figure S24. Images of Petri dishes revealing the antibacterial activity of **4** against *S. aureus*.

Supporting References

S1. J. S. Chickos and A. Gavezzotti, *Cryst. Growth Des.,* 2019, **19**, 6566-6576.

S2. G. Bardi, L. Bencivenni, D. Ferro, B. Martini, S. Nunziante Cesaro and R. Teghil, *Thermochim. Acta.* 1980, **40**, 275-282.

S3. J. S. Chickos and W. E. Jr. Acree, *J. Phys. Chem. Ref. Data.* 2002, **31**, 537-698.

S4. M. Kumar, G. Jaiswar, M. Afzal, M. Muddassir, A. Alarifi, A. Fatima, N. Siddiqui, R. Ayub, N. A. Y. Abduh, N. A. Y., W. S. Saeed and S. Javed, *Molecules*, 2023, **28**, 2116.

S5. M. Graindourze, T. Grootaers, J. Smets, T. Zeegers-Huyskens and G. Maes, *J. Mol. Struct.* 1990, **237**, 389-410.

S6. H. F. Roenfanz, T. J. Paniak, C. B. Berlin, V. Tran, K. R. Francisco, P. Lassalas, A. Devas, O. Landes, A. Rosenberger, M. E. Rotella, C. Ballatore and M. C. Kozlowski, *Chem. Eur. J.* 2023, **29**, e202300696.